NASA Technical Memorandum 83369

Time Effect of Erosion by Solid Particle Impingement on Ductile Materials

P. Veerabhadra Rao and Donald H. Buckley
Lewis Research Center
Cleveland, Ohio

Prepared for the
Sixth International Conference on Erosion by Liquid and Solid Impact
sponsored by the Cavendish Laboratory (University of Cambridge)
Cambridge, England, September 4–8, 1983

NASA

TIME EFFECT OF EROSION BY SOLID PARTICLE IMPINGEMENT ON DUCTILE MATERIALS

P. Veerabhadra Rao and Donald H. Buckley

National Aeronautics and Space Administration
Lewis Research Center
Cleveland, Ohio 44135

E-1592

Several metals and alloys were eroded by jet impingement of glass beads and crushed-glass particles in order to investigate the influence of exposure time on volume loss rate. The results indicate a direct relation between erosion-versus-time curves and pit morphology (width, depth, and width-depth ratio) for impingement with both glass forms. Analysis of the present experimental data showed four types of erosion-rate-versus-time curves: (1) incubation, acceleration, and steady-state periods (type I), (2) incubation, acceleration, deceleration, and steady-state periods (type III), (3) incubation, acceleration, peak rate, and deceleration periods (type IV), and (4) incubation, acceleration, steady-state, and deceleration periods (type V). Type IV and V curves are less frequently seen and have not been reported in the literature. An analysis of extensive erosion data in the literature generally indicated three types of erosion-rate-versus-time curves. Two of these (types I and III) were observed in the present study; the third type involves incubation (and deposition), acceleration, and steady-state periods (type II). Data analysis indicated that the corresponding stages, or periods, of erosion must be considered in parametric studies correlating and characterizing erosion resistance of a wide spectrum of ductile materials. The erosion rates of materials can be predicted by using the incubation period intercepts from the linear portion of erosion-versus-time curves.

INTRODUCTION

Solid-particle impingement erosion confronts the design engineers of land-based coal gasification machinery for energy generation and conversion and operational aircraft such as all-weather helicopters, which must operate in dusty environments, or aircraft that must land on unprepared airstrips. The detrimental effects of damage and erosion on the material surfaces of various components used in the petrochemical, aircraft, and coal gasification industries are mainly governed by the function, performance, and efficiency necessary for a particular component. In some systems or components even the smallest amount of damage or embedment cannot be tolerated (e.g., optically guided systems and radomes). Other components function with loss of efficiency until they break down completely (e.g., components of coal gasification systems).

Cyclones in coal gasification plants generally remove most of the large particles that cause major erosion, leaving particles smaller than 20 μm. Those particles also cause considerable damage and erosion to the turbine stator and rotor blades, valves, bends, pipelines, etc., in coal-burning plants (1-5). An energy conversion plant is expected to operate for 20 000 hours without a major costly breakdown (1). It has been, however, estimated that components such as stator and rotor blades of a coal-burning turbine have maximum lives of 5000 and 10 000 hours, respectively (6), due to erosion. Failures of these components can cause long and unanticipated shutdowns for the entire powerplant. A recent compilation (1) clearly states the importance of erosion and related component failures in energy conversion systems.

Helicopter rotor blades have a total life of approximately 10 hours under severely erosive conditions such as dust clouds when particle concentrations of 10 mg m^{-3} are encountered (7,8). Even shorter exposures and erosion-related failures have been mentioned by Hibbert (7). For example, a main rotor blade of a helicopter was eroded and split open after 2-1/2 hours of flight in a dust cloud. A tail rotor blade made of an aluminum alloy was eroded through after just 1 hour of operation in the ground cushion (7); a stainless-steel blade lasted only 1-1/2 hours. Montegomery and Clark (9) present a graph to estimate the life of centrifugal helicopter engines that considers both erodent particle size and dust concentration. Despite the use of filters - ordinary and centrifugal cyclone types - for helicopter engine compressors, the ultimate efficiency of the system controls the overall erosion process (7,10).

The main purpose of testing materials has been to understand the erosion mechanism in general and to characterize the erosion resistance of materials in particular for a variety of applications: Knowing the effect of exposure time or abrasive charge on weight loss or erosion rate is essential not only to understanding precisely the different stages, or periods, of erosion with time for correlation and characterization purposes, but also to modeling and extrapolating laboratory data more precisely to field conditions. For long-term exposure to erosive environments the ef-

fect of time on erosion rate is of paramount importance in estimating the true expected lives of the components. Most of the earlier estimates have been made on the assumption of a constant erosion (steady state) rate for long-term exposures. A recent study (11), however, indicates that erosion rate drops off for prolonged exposures with sharp-edged (angular) particles, the particles generally encountered in field situations.

The effect of time or particle charge on the mass loss of different materials has been studied since the 1950's (12-14). Only recently, however, have the different erosion stages, or periods, been precisely defined, contributing to the meaning of the erosion stage (1,2,11).

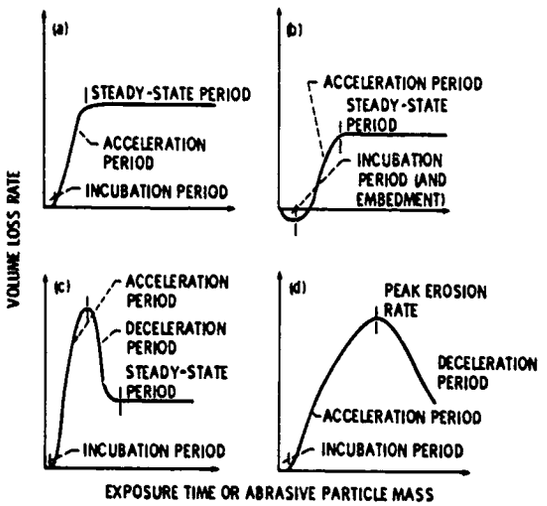

(a) Type I. (b) Type II.
(c) Type III. (d) Type IV.

Figure 1. - Characteristic volume-loss-rate-versus-time curves.

Fig. 1 is a schematic representation of the volume-loss-rate-versus-time curves for the typical cumulative-mass-loss-versus-time or abrasive dosage plots generally found in the literature (11). In this paper the curves in Fig. 1 are referred to as type I, II, III, and IV, and their trends are shown in the figure. In general, the solid-particle impingement erosion process on ductile metals can be characterized by the following stages, or periods.

(1) Incubation or induction period, the time span or dosage of erodent particle mass during which there is little or no weight loss. In fact, in a few cases there can be a slight weight gain due to the embedment or adhesion of particles.

(2) Acceleration or accumulation period, the time span in which the weight loss rate increases rapidly

(3) Deceleration or attenuation period, the time span representing rapidly decreasing weight loss rate

(4) Steady-state period, the time span in which the weight loss rate becomes constant and continuous for a long time. This is the period commonly referred to as the "maximum rate" or "constant rate" period. (Sometimes for long-term exposures, erosion rates become lower than the peak erosion rate, Fig. 1(c).)

(5) Peak erosion rate, the maximum erosion rate observed between the acceleration and deceleration periods, Fig. 1(d).

Most of the investigators have discussed erosion-rate-versus-time curves that contain incubation, acceleration, and steady-state periods, such as shown in Figs. 1(a) and (b). However, a typical erosion-rate-versus-time curve, as in Fig. 1(c), has been presented in (11,15) and also discussed in (1,16). Although the curves in Figs. 1(c) and (d) are less frequently seen, they have practical significance.

Most previous tests of solid-particle impingement erosion were continued until the maximum rate of erosion was established (2). This was accomplished by running the test for successive equal time steps and obtaining the same value of weight loss for each of these steps. A systematic study, however, to understand and to compare the effect of time on erosion rate for different materials with various types of particles and experimental devices had not previously been undertaken, other than by the present authors (11). A literature survey of the time effects on erosion rate and on the different types of curves in Fig. 1, covering different types of particles, devices, experimental conditions, etc., has recently been presented (11). The goal of understanding the erosion process for an aluminum alloy further motivated the present study.

The present paper reports erosion-rate-versus-time curves for several metals and alloys undergoing glass-bead and crushed-glass jet impingement at normal incidence. The study of pit morphology (the width, depth, and width-depth ratio of pits) with the use of the scanning electron microscope (SEM) provided a very good insight into the erosion-rate-versus-time curves. This paper (1) considers the necessity of using corresponding periods of the erosion-rate-versus-time curves to compare and correlate erosion data with material properties in order to achieve meaningful parametric studies and characterization of the erosion resistance of materials and (2) predicts erosion rate as a function of intercept. This paper is, in part, a condensed version of (11).

NOMENCLATURE

A	coefficient
a	coefficient
b	coefficient
c	coefficient
d	depth of the pit
m	exponent
N	exponent
n	exponent
R	correlation coefficient
t_i	incubation period intercept
V	particle velocity
w	width of the pit

APPARATUS AND EXPERIMENTAL PROCEDURE

Specimens

Specimens of copper, cobalt, nickel, aluminum alloy 6061-T6511, brass, 1045 steel, 304 stainless steel, 4340 steel, 1010 steel, and tool steel were used in this investigation. All specimens were 6 mm thick, 25 mm wide, and 37.5 mm long, except for 1045 steel specimens, which were 6 mm thick and 25.4 mm in diameter. The latter were tested on the flat surface. The nominal composition and mechanical properties of the metals and alloys are available in (17). Before erosion exposure all specimens were polished with 600-grit emery paper and then with 3-μm diamond paste, cleaned with distilled water, and air dried.

Apparatus and Procedure

Commercial grade no. 9 spherical glass beads of approximately 20-μm average diameter and commercial grade no. 10 crushed glass of 30-μm size were used. The particle size distribution of glass beads is discussed in (18). The SEM micrographic details of the sizes and shapes of both forms of glass are available in (19,20).

A sandblasting facility was used to continuously impact test specimens with erodent particles at normal incidence. A schematic of the sandblasting nozzle arrangement can be found in (11,18). The distance between the specimen and the nozzle (1.18 mm diam) was 13 mm. The stagnation pressure of the argon driving gas was varied from 0.13 to 0.82 MPa (gage) pressure. The average particle velocities are presented in Table 1. The

TABLE 1. - PARTICLE VELOCITY OF GLASS BEADS AND CRUSHED-GLASS PARTICLES

Erodent	Particle velocity for following jet gas pressures, (MPa), m s^{-1}					
	0.14	0.27	0.41	0.54	0.68	0.82
Glass beads	52	72	87	101	113	130
Crushed glass	41	48	60	68	76	87

velocities are obtained by using a double disk arrangement similar to one discussed earlier (21). The jet divergence was about ±2° relative to the centerline. The nozzle was replaced frequently during the experiments, and this limited the effect of nozzle wear on jet divergence, impingement velocity, erodent flow rate, etc.

Volume loss values were obtained by weighing specimens before and after their exposure to both forms of glass and dividing by density. The detailed information pertaining to the experimental data scatter and standard deviation can be found in (18,19). The sensitivity of the balance was 0.1 mg. Surface profiles of the eroded surfaces were recorded with a profilometer. The depths of the shallow pits were measured from surface traces and checked with a depth gage. The deep pits were always measured with a depth gage. The sensitivity of the gage was ±2.5 μm (0.0001 in.). The eroded surfaces were observed with an SEM.

EXPERIMENTAL RESULTS AND DISCUSSION

Erosion-Rate-Versus-Time Curves

Spherical particle impingement. - A typical cumulative-volume-loss-versus-time curve and the instantaneous-volume-loss- rate-versus-time curve of an aluminum alloy specimen exposed to glass-bead jet impingement at a pressure of 0.27 MPa are presented in Fig. 2.

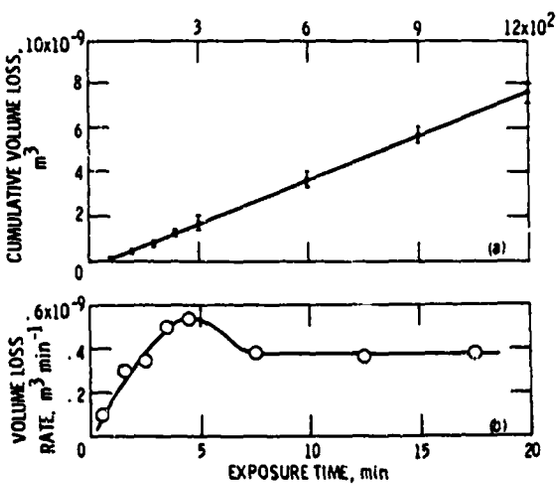

(a) Volume loss.

(b) Volume loss rate.

Figure 2. - Typical erosion-versus-time curves. Pressure, 0.27 MPa; glass bead flow rate, 0.98x10^{-3} kg s^{-1}.

The instantaneous volume loss was calculated as the slope of the local tangent (Fig. 2(a)). Fig. 2(b), which is similar to Fig. 1(c), is a type III curve consisting of four zones (incubation, acceleration, deceleration, and steady state). As mentioned earlier, this type of curve has been discussed for stainless steel and copper in the literature (1,15,16).

Comparisons of Fig. 2(b) with the curves of total width, rate of width, total depth, rate of depth, and width-depth ratio of pits as a function of exposure time in Fig. 3 provide a good insight into the erosion process. The initial spike of the erosion rate is believed to be due to the rapidly increasing width, depth, and width-depth ratio of the pit with time. The glass-bead flow rate was highest at 0.27 MPa, and this may also be responsible for the initial peak rate of erosion, or spike.

It is easy to suspect the influence of periodic impingement (testing specimen at specified intervals of time) and the statistical variation of the experimental data on the observed initial spike. A systematic study to determine the effect of periodic impingement on the erosion-rate-versus-time curves of metals and plastics revealed similarity in

erosion characteristics to those generally occurring in airblasting (22). However, present studies indicate an increased erosion for long periodic exposures. Extensive data analyzed by the authors indicate that the standard deviation of the experimental data is less pronounced than the trend of the curve. Hence, it can be assumed that the volume-loss-rate-versus-time curve observed is a characteristic of pit morphology and related influences rather than a result of periodic impingement and experimental data variation.

It was observed that pit-width-versus-time or pit-depth-versus-time curves approximately represent erosion-versus-time curves but to a different scale during jet impingement (11). Under different experimental conditions (15) measurements of specimen weight loss and erosion crater (pit) depth as a function of abrasive flow have shown a complicated relationship. It was further evident from (11) that as the width-depth ratio of the pit ceases to increase with time, the erosion rate attains a steady state (Fig. 3(d)).

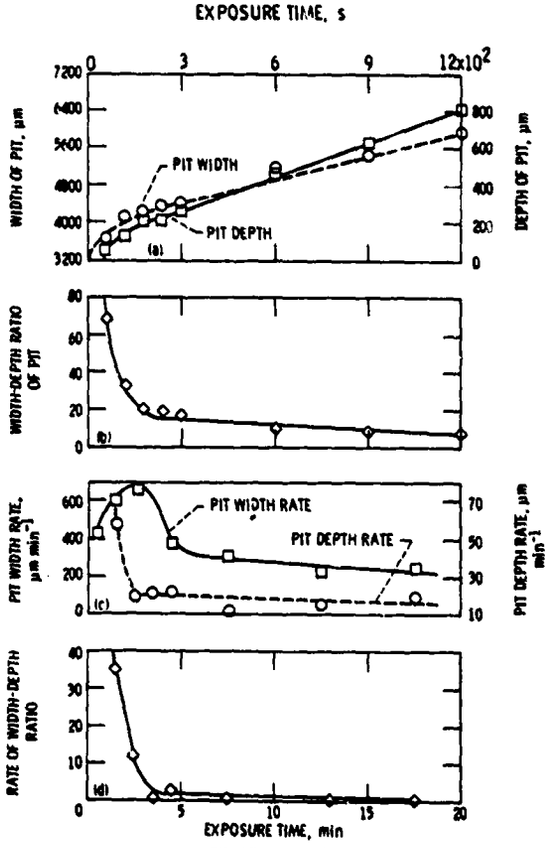

(a) Pit width and pit depth.
(b) Width to depth ratio of pit.
(c) Growth rate of pit width and pit depth.
(d) Growth rate of width to depth ratio of pit.

Figure 3. - Width, depth, and width-depth ratio of pit as a function of exposure time.

Fig. 4 presents typical instantaneous erosion-rate-versus-time curves of an aluminum alloy at pressures from 0.41 to 0.82 MPa (gage) during glass-bead jet impingement. The solid lines in Fig. 4 represent the least-

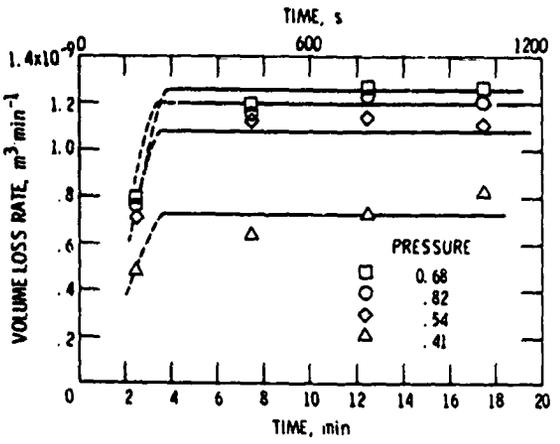

Figure 4. - Instantaneous volume loss rate versus time curves of aluminum alloy at different pressures during glass-bead impingement.

squares-fit slope obtained at each pressure condition. The curves in this figure exhibit only acceleration and steady-state periods similar to those of type I curves (Fig. 1(a)). Analyses of erosion data on aluminum impacted with spherical particles (11) resulted in curves identical to these. Other investigators using both spherical (11) and angular particles (4,12-14), also discussed similar weight-loss-versus-abrasive-charge curves.

As the pressure of the jet increased, the width-depth ratio of the pit reached a limiting value. From the morphological studies (19) it is evident that both the appearance of "radial concentric rings" inside the pit and platelet removal approximately coincide with the "steady state" erosion rate period.

Rickerby and Macmillan (23) state that after erosion begins, an ever-decreasing amount of additional strain hardening takes place as subsequent impacts harden and reduce the extent of those areas not yet fully hardened. This condition gradually increases the extent of platelet formation and causes the erosion to attain its steady-state value.

Crushed-glass impingement. - Fig. 5 presents typical cumulative erosion and instantaneous-erosion-rate-versus-time curves for brass, 1010 steel, and tool steel specimens impacted with a jet of crushed-glass angular particles at a pressure of 0.54 MPa. The curves in Fig. 5(b) are different from those in Figs. 1(a) to (c) and were neither discussed nor reported other than by Rao and Buckley (11). Analysis of extensive data on various materials eroded by different sizes of angular particles resulted in types I to III curves in most cases (11). A typical set of instantaneous-erosion-rate-versus-time curves of an aluminum alloy impinged at pressures from 0.14 to 0.82 MPa is presented in Fig. 6. The curves in this figure exhibit only acceleration, peak erosion, and deceleration periods similar to those of type IV curves (Fig. 1(d)). Type IV curves are less frequently seen. Erosion-rate-versus-time curves for 1010 steel and tool steel have acceleration, steady-state, and deceleration periods. This curve is of still another type and is also less frequently observed.

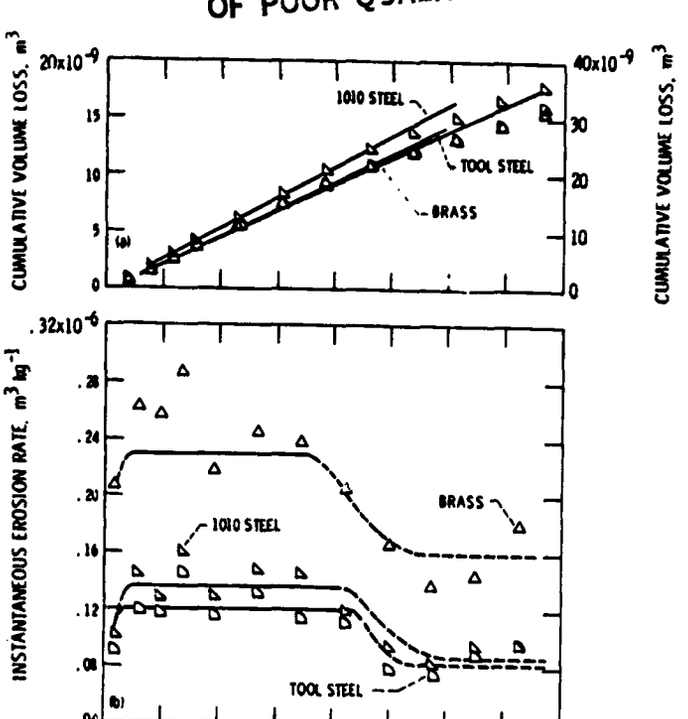

(a) Volume loss.
(b) Volume loss rate.

Figure 5. - Typical erosion-time curves during crushed-glass impingement. Pressure, 0.54 MPa; crushed-glass flow, 0.26×10^{-3} kg s^{-1}.

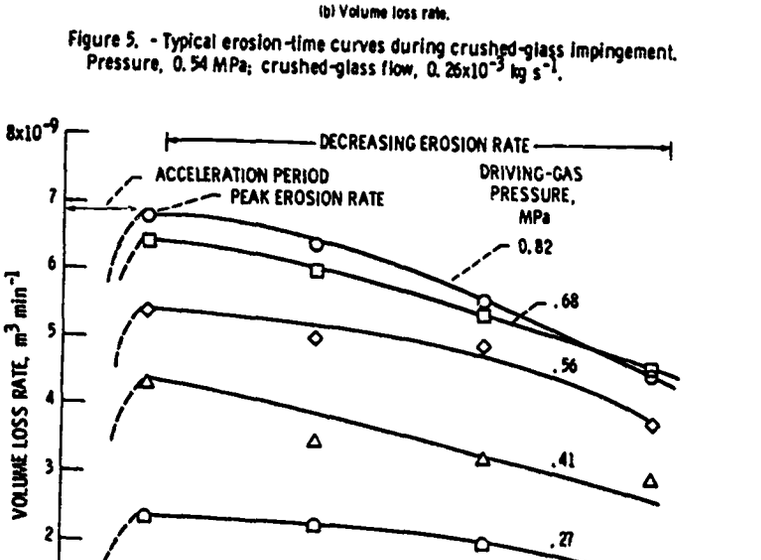

Figure 6 - Instantaneous volume-loss-rate-versus-time curves of aluminum alloy at different pressures during crushed-glass particle impingement.

Table 2 presents typical pit parameters, namely, depth, width, and width-depth ratio, of different materials. A comparison of depth, width, and width-depth ratio of pits with erosion indicates that pit-depth-rate-versus-time curves are similar to erosion-rate-versus-time curves (11). Pit-width-rate-versus-time and width-depth-ratio-versus-time curves decelerate faster than erosion-rate-versus-time curves.

At long exposure times the depth of the pit may become sufficient to affect the erosion rate. A similar possibility is mentioned in (15). This produces two effects:

TABLE 2. - PIT PARAMETERS FOR VARIOUS MATERIALS DURING CRUSHED-GLASS IMPINGEMENT

Exposure time, min	Pit parameter	Values of pit parameters for the material -						
		Aluminum alloy 6061-T6511	Brass	1045 Steel	304 Stainless steel	4340 Steel	1010 Steel	Tool steel
0.5	Width, w, μm	4660	5020	4665	4645	4555	4220	4330
	Depth, d, μm	414	551	277	396	251	251	229
	w/d	11.3	9.1	16.8	11.7	18.1	16.8	18.9
1	Width, w, μm	5730	5880	5175	5510	5620	5110	5060
	Depth, d, μm	864	1064	518	699	495	561	508
	w/d	6.6	5.5	10	7.9	11.4	9.1	10
1.5	Width, w, μm	6000	5960	5550	5665	5955	5220	5380
	Depth, d, μm	1300	1458	711	991	615	833	762
	w/d	4.6	4.1	7.8	5.7	9.7	6.3	7.1
2	Width, w, μm	6000	6300	5730	6045	6300	5620	5550
	Depth, d, μm	1966	1872	970	1293	874	1123	1041
	w/d	3.1	3.4	5.9	4.7	7.3	5.0	5.3
3	Width, w, μm	6050	6400	6085	6420	6330	5730	5730
	Depth, d, μm	2416	2629	1478	1902	1369	1603	1486
	w/d	2.5	2.4	4.1	3.4	4.6	3.6	3.9
4	Width, w, μm	6200	6400	6330	6485	6710	5870	5890
	Depth, d, μm	3089	3213	1918	2324	1852	2126	1948
	w/d	2	2	3.3	2.8	3.6	2.8	3.0
5	Width, w, μm	6620	6770	6440	6890	6880	6010	5910
	Depth, d, μm	3647	3752	2253	2400	2172	2469	2141
	w/d	2.1	1.8	2.9	2.9	3.2	2.4	2.8
6	Width, w, μm	6890	6840	6440	—	—	6220	6240
	Depth, d, μm	4074	4140	2578	—	—	2817	2593
	w/d	1.7	1.7	2.5	2.3	2.7	2.2	2.4
7	Width, w, μm	6890	6910	—	6890	6930	6400	6880
	Depth, d, μm	4442	4617	—	3167	2847	3127	2807
	w/d	1.6	1.5	2.4	2.2	2.4	2	2.5
8	Width, w, μm	6900	6950	6575	6930	6930	6400	6950
	Depth, d, μm	4796	4864	3172	3385	3167	3360	3155
	w/d	1.4	1.4	2.1	2	2.2	1.9	2.2
9	Width, w, μm	6900	6950	6840	—	6960	6400	6950
	Depth, d, μm	4874	4953	3426	—	3269	3498	3241
	w/d	1.4	1.4	2	1.9	2.1	1.8	2.1
10	Width, w, μm	6900	6950	—	—	—	6440	6950
	Depth, d, μm	5085	5011	—	—	—	3686	3360
	w/d	1.5	1.4	—	—	—	1.7	2.1

(1) an increase in the distance between the specimen and the jet nozzle and (2) decreasing jet velocity along the jet. Both of these effects reduce erosion rate (21,24).

Once the pit is very deep, the momentum of the jet has to almost reverse to push the particles out of the pit. Because of the confined nature of the pit the jet may be cushioned or shielded by a layer of particles at the bottom of the pit. This can reduce the erosion rate in some situations.

DATA ANALYZED FROM THE LITERATURE

In order to understand the general nature of the different types of erosion-rate-versus-time curves with reference (1) to particle size and shape (angularity) and (2) to impact velocity, extensive erosion data were analyzed systematically (11). The main conclusions from this analysis are (1) that most curves conform to the type I and II curves (Figs. 1(a) and (b)) when a smooth curve is drawn through the experimental points and (2) that some curves of the present investigators and of others occasionally conform to type III and IV curves (Fig. 1(c) and (d)).

Angular particles caused maximum deposition at normal incidence angle; deposition, however, increased with decreasing velocity and decreasing particle size with slight exceptions. Spherical particles generally did not cause deposition or embedment. Hence, it may be surmised that with angular particles at normal incidence there is every possibility that erosion-rate-versus-time curves will conform to the type II curve (Fig. 1(b)). When embedment took place, the steady-state erosion rate did not vary much in most situations. For angular particle impingement the incubation and acceleration periods were short compared with those obtained with spherical particles.

As impact velocity decreased, the scatter decreased and the erosion-rate-versus-time curve stabilized. Higher impact velocities exhibited scatter and resulted in type IV erosion rate-versus-time curves (Fig. 1(d)). As velocity decreased, deposition of particles increased and the erosion process began. Hence, the incubation and acceleration periods were long.

Because five types of erosion-rate-versus-time curves (types I to V, Figs. 1 and 5(b)) were observed under vastly different experimental conditions, it is essential to consider a steady-state region or a peak erosion rate in any parametric study characterizing and comparing experimental results for a wide spectrum of ductile materials. Large

variations in the magnitude of erosion in the laboratory as well as in field situations suggest that test results should be compared only on the basis of corresponding stages and periods of the erosion-rate-versus-time curves. If this is not done, it is the present authors' opinion that scaling and modeling of erosion may not be precise and may result in errors.

Testing of various materials with a criterion of a fixed time interval is not the correct procedure for characterizing and modeling efforts. Erosion-rate-versus-abrasive-charge curves on different materials (Figs. 2(b) and 5(b)) would certainly reinforce this concept. To show an example of the influence of time on a parametric study, erosion-rate-versus-particle-velocity plots obtained during the glass-bead impact erosion of copper specimens are presented in Fig. 7. These plots

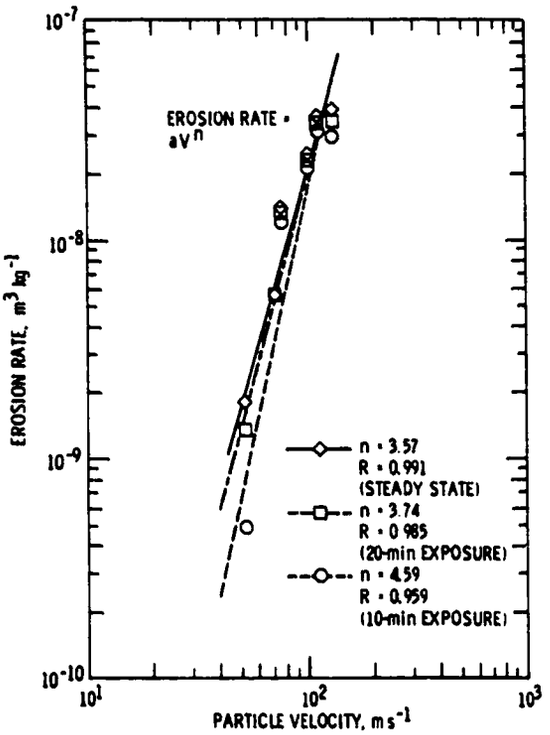

Figure 7. - Normalized erosion rate as a function of particle velocity illustrating the effect of stage of erosion.

represent 10-min, 20-min, and steady-state erosion rates. During the acceleration stages of erosion the exponents obtained in the relation (erosion rate is proportional to velocity) are very high. However, for the correlation during the steady-state region the velocity exponent value agrees with the exponent obtained on the aluminum alloy (19) for steady-state erosion rate correlation with jet flow velocity.

In order to arrive at a steady-state period, the material specimen should be tested at equal time intervals to obtain an approximately constant volume loss. On the other hand, if there is considerable deviation of volume loss rate when a metal is tested at fixed time intervals, the entire history of the erosion-versus-time curves should be obtained. It is observed in Fig. 2(b) and in (11,15) that a spike in erosion rate (similar to Fig. 1(c)) is 150 to 300 percent higher than the steady-state erosion rate. Hence, the use of corresponding periods, or stages, of erosion in parametric studies correlating and characterizing different materials is justified.

INCUBATION PERIOD

The incubation period (with or without embedment) poses a lot of problems in changing friction and drag (including optical transmittance) characteristics of surfaces

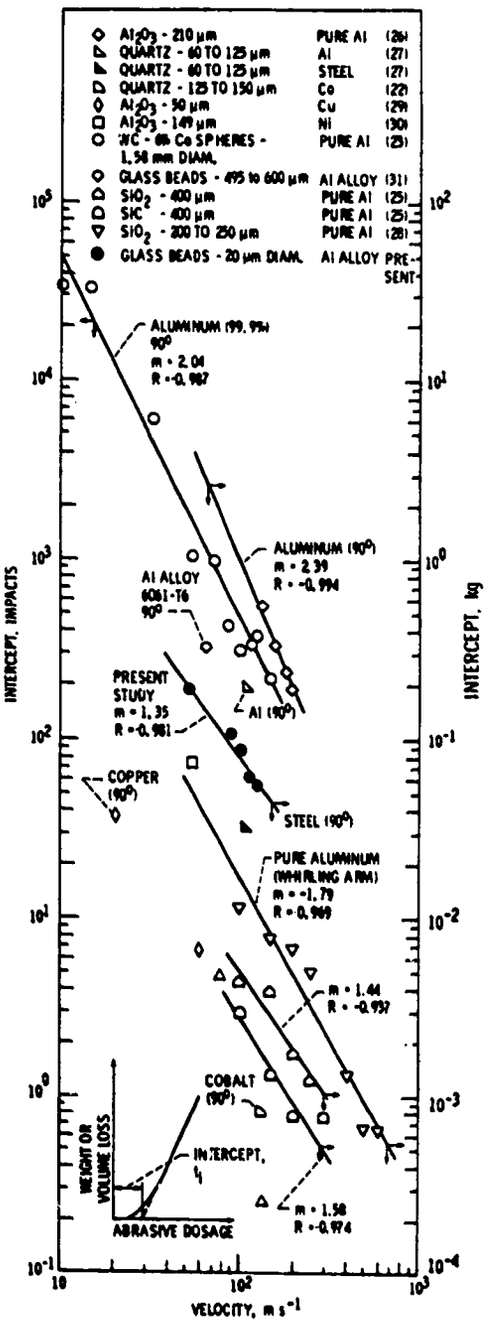

Figure 8. - Intercept as a function of particle velocity.

because of damage caused by the impingement. Hence, an approximate estimate of the magnitude of this period provides not only the duration of damaged-surface impact encounters but also the time and severity of particle embedment. The optical degradation of aircraft canopies and windshields further reemphasizes the necessity for this type of study. Fig. 8 presents the intercept (see schematic representation) versus particle velocity for aluminum alloy surfaces impinged with glass beads. The exponent m obtained by using least-squares fit with a relation

$$t_i = bV^{-m} \qquad (1)$$

is 1.35.

To establish the variation of exponents on several ductile materials, Fig. 8 was also plotted for normal impact data from the literature (22,23,25-31) for several materials. This figure indicates both exponent m and correlation coefficient R for each data set. The values of m vary from 1.35 to 2.4. Most of the data for other materials also follow the same trend. The theoretical analysis by Hutchings (31) indicates an exponent of m = 2; his experimental data indicate m = 1.9. However, there seems to be a strong influence of size, shape (angularity), and concentration of particles and type of experimental configuration on the intercept. As the size increased, the values of m decreased for aluminum impacted with angular particles irrespective of the type of device. The situation seems to be reversed, however, for spherical particles (Fig. 8).

PREDICTION OF EROSION RATE

Erosion rate has always been expressed as

$$\text{Erosion rate} = aV^n \qquad (2)$$

Similarly, it has been proven that intercept t_i (Fig. 8) can also be expressed in terms of V as shown in Eq. (1). Substituting Eq. (1) in Eq. (2) results in

$$\text{Erosion rate} = a(b/t_i)^{n/m} = c/t_i^{n/m} \qquad (3)$$

or

$$\text{Erosion rate} = (a/b)t_i V^{n+m} \qquad (4)$$

Eqs. (3) and (4) indicate a direct relation between erosion rate and intercept. Table 3 presents exponents n, m, and n/m ratio for aluminum alloy tested by the present authors and by other investigators (13,23,25,26,28, 29). Data pertaining to pure aluminum, copper, and Nimonic 80A alloy were also presented to check the validity of this prediction attempt. Aluminum and Nimonic alloy were examined in a rotating-arm device. The analysis of data presented in Table 3 establishes that erosion rates of materials can be predicted by using the intercepts or incubation periods under identical conditions. This is interesting because it is easy to establish the exponents n and m of a particular material and this then predicts erosion rate reasonably well. It is, however, necessary to assess the advantage of this method over material and other property correlations with erosion rates. Eq. (3) appears to be empirical. If the analysis advanced by Hutchings (31) is incorporated, it becomes dimensionally stable, but theoretical analysis results in erosion rate proportional to $t_i^{-1.5}$.

It is further observed that it is possible to predict total erosion volume using

TABLE 3. - PREDICTION OF EROSION RATES WITH INTERCEPTS

[Erosion rate = $c/t_i^{n/m}$.]

Investigators	Material	Type of device	Particle size	n	m	n/m	Remarks
Neilson and Gilcrist (26)	Aluminum	Jet	210-μm Al_2O_3	3.15	2.39	1.32	———
Rickerby and Macmillan (23)	Al(99.9 percent pure)	Rotating arm	1.58-mm-diam WC - 6 percent Co spheres	3.3	2.04	1.62	———
Ives and Ruff[a] (29)	Cu OFHC (ASTM B170 grade 1)	Jet and specimen rotating	50-μm Al_2O_3	2.52	1.59	1.58	———
Duffin[a] (13)	Nimonic 80A	Whirling arm	50-μm feldspar	1.73 2.66	4.08 3.67	.42 .72	20° C 400° C
Kayser[a] (25)	Pure Al	Whirling arm	400-μm SiO_2 400-μm SiC	1.06 1.36	1.44 1.58	.74 .86	——— ———
Behrendt (28)	Pure Al	Whirling arm	200- to 250-μm SiO_2	2.9	1.79	1.62	———
Present	Al 6061-T6	Sandblasting	20-μm glass beads	3.67	1.35	2.72	———

[a]Equations used are $(\text{Erosion rate})_1/(\text{Erosion rate})_2 = (V_1/V_2)^n$

$(\text{Intercept})_1/(\text{Intercept})_2 = (V_1/V_2)^{-m}$

$(\text{Erosion rate})_1/(\text{Erosion rate})_2 = (\text{Intercept})_1/(\text{Intercept})_2^{-n/m}$

TABLE 4. - PREDICTION OF EROSION VOLUME WITH PIT PARAMETERS[a]

Erodent	Constant A, exponent N, and correlation coefficient R in the relationship Erosion volume = A (pit parameter)^N for the pit parameter								
	Pit width, w, μm			Pit depth, d, μm			Width-depth ratio of pit		
	A	N	R	A	N	R	A	N	R
Glass beads	4.69×10^{-24}	6.43	0.987	9.10×10^{-4}	1.29	0.991	113.06	-1.60	-0.987
Crushed glass	2.30×10^{-22}	6.05	.962	1.77×10^{-2}	1.20	.995	84.03	-1.51	-.993

[a]Experimental data were computed for 6061-T6 aluminum alloy tested at pressures, 0.14, 0.27, 0.41, 0.54, 0.68, and 0.82 MPa using both glass beads and crushed glass particles. The relationships used for computations were
Erosion volume = A (pit width)^N
Erosion volume = A (pit depth)^N
Erosion volume = A (width-depth ratio of pit)^N

the depth, width, and width-depth ratio of the pit for 6061-T6 aluminum alloy surfaces impacted with both forms of glass at different pressure conditions. The resulting relations and correlation coefficients are presented in Table 4. The depth and width-depth ratio of the pit predict volume loss better than the width of the pit (Table 4).

CONCLUSIONS

(1) Studies with jets of glass beads and crushed-glass particles resulted in four types of erosion-rate-versus-time curves: (1) incubation, acceleration, and steady-state periods (type I), (2) incubation, acceleration, deceleration, and steady-state periods (type III), (3) incubation, acceleration, peak rate, and deceleration periods (type IV), and (4) incubation, acceleration, steady-state, and deceleration periods (type V). Type IV and V curves are rare shapes of erosion-rate-versus-time-curves and have not been reported by other researchers.

(2) The pit-width-versus-time or pit-depth-versus-time curves were similar to the cumulative-erosion-versus-time curves for glass-bead impingement. The pit-depth-rate-versus-time curves were similar to the erosion-rate-versus-time curves for crushed-glass impingement. In both cases the pit morphology (width, depth and width-depth ratio) strongly controlled the erosion-rate-versus-time curves.

(3) Analysis of a large amount of data from the literature indicated that under different experimental conditions three types of erosion-rate-versus-time curves emerge. Two types (types I and II) were observed in the present investigation, and the third type involves incubation (and deposition), acceleration, and steady-state periods (type II). With angular particles at a normal angle of incidence erosion-rate-versus-time curves conform to the type II curve (Fig. 1(b)).

(4) The incubation and acceleration periods increased with decreasing impact velocity and decreased when angular particles were used instead of glass beads.

(5) Analysis of the present experimental results and data presented in the literature provided an understanding that the corresponding stages, or periods, of erosion must be considered in parametric studies correlating and characterizing the erosion resistance of different materials. The erosion rates of materials can be predicted with sufficient accuracy by using incubation period intercepts obtained from the linear portion of the erosion-versus-time curves.

REFERENCES

1. National Materials Advisory Board 1977, NMAB-334, Washington, D.C.
2. Adler W. F. 1979, Rept. ETI CR-79-680, U.S. Army Research Office.
3. Ruff A. W. and Wiederhorn S. M. 1979, NBSIR 78-1575, National Bureau of Standards.
4. Tilly G. P. 1979, in "Treatise on Materials Science and Technology" (Scott D., ed.) Academic Press 1979, p. 287.
5. Schmitt G. F. Jr. 1980, in "Wear Control Handbook" (Peterson M. P. and Winer W. O., eds.) American Society of Mechanical Engineers, p. 231.
6 Nabors W. M., Strimbeck, D. C., Cargill, R. W., and Smith, J. 1965, J. Eng. Power. 87, 215.
7 Hibbert W. A. 1965, J. R. Aeronaut. Soc., 69, 769.
8 Goodwin, J. E., Sage W. and Tilly G. P. 1969-70, Proc. Inst. Mech. Eng. London 184, 279.
9. Montegomery J. E. and Clark J. M. 1962, SAE Paper 538 A.
10. Sage W. and Tilly G. P. 1969, J. R. Aeronaut. Soc. 73, 427.
11. Rao P. V. and Buckley D. H. 1983 NASA TP-2169. National Aeronautics and Space Administration.
12. Finnie I. 1958, Proc. 3rd Nat. Cong. of Appl. Mech. New York, American Society of Mechanical Engineers, 527.
13. Duffin H. C. 1960, Nat. Gas Turbine Establishment Memo. No. M. 341.
14. Finnie I., Wolak J. and Kabil Y. 1967, J. Mater. 2, 682.
15. Young J. P. and Ruff A. W. 1977, J. Eng. Mater. Technol. 99, 121.
16. Follansbee P. S., Sinclair G. B. and Williams J. C. 1981-82, Wear 74, 107.

17. Lyman T. ed. 1961 Metals Handbook, Vol. 1, 8th ed. American Society for Metals.
18. Rao P. V., Young S. G. and Buckley D. H. 1983, NASA TP-2161. National Aeronautics and Space Administration.
19. Rao P. V., Young S. G. and Buckley D. H. 1983, Wear 85, 223.
20. Salik J. and Buckley D. H. 1981, NASA TP-1755, National Aeronautics and Space Administration.
21. Ruff A. W. and Ives L. K. 1975, Wear 35, 195.
22. Tilly G. P. and Sage W. 1969, ASME Paper No. 69-WA/Met-6.
23. Rickerby D. G. and Macmillan N. H. 1980, Wear 60, 369.
24. Wolak J., Worm, P., Patterson, I. and Bodoia, I. 1977, J. Eng. Mater. Technol. 99, 147.
25. Kayser W. 1967, Proc. 2nd Meersburg Conf. on Rain Erosion, Meersburg, 1967, Royal Aircraft Establishment, 427.
26. Neilson J. H. and Gilchrist A. 1968, Wear 11, 111.
27. Tilly G. P. 1969, Wear 14, 63.
28. Behrendt A. 1970, Proc. 3rd Int. Conf. on Rain Erosion and Associated Phenomena. England, 1970, Royal Aircraft Establishment, 2. 797.
29. Ives L. K. and Ruff A. W. 1977, in "Erosion: Prevention and Useful Applications" (Adler W. F. ed.) ASTM, p. 5.
30. Kosel T. H., Scattergood R. O. and Turner A. P. L. 1979, in "Wear of Materials 1979" (Ludema K. C., Glaeser W. A. and Rhee S. K, eds.) ASME, p. 192.
31. Hutchings I. M. 1981, Wear 70, 269.

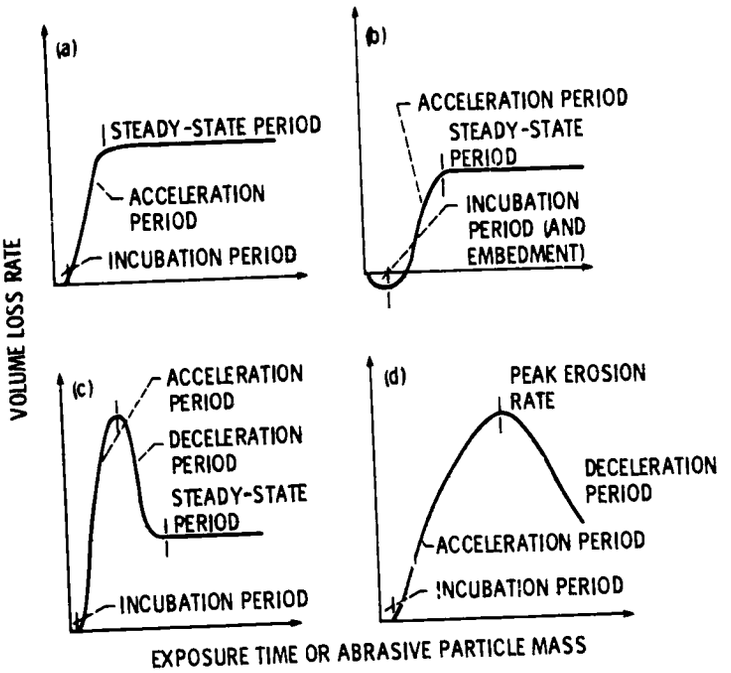

(a) Type II.
(b) Type III.
(c) Type I.
(d) Type IV.

Figure 1. - Characteristic volume-loss-rate-versus-time curves.

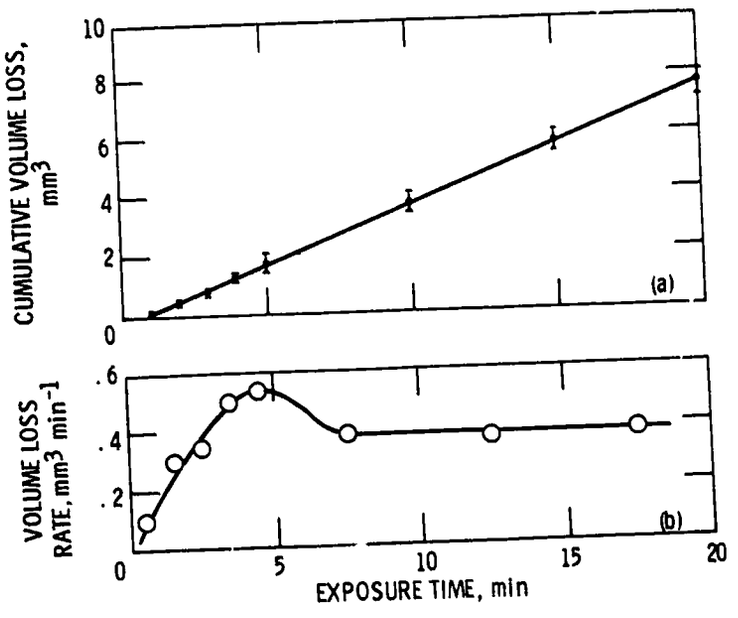

(a) Volume loss.
(b) Volume loss rate.

Figure 2. - Typical erosion-versus-time curves. Pressure, 0.27 MPa; glass bead flow rate, 0.98 g sec^{-1}.

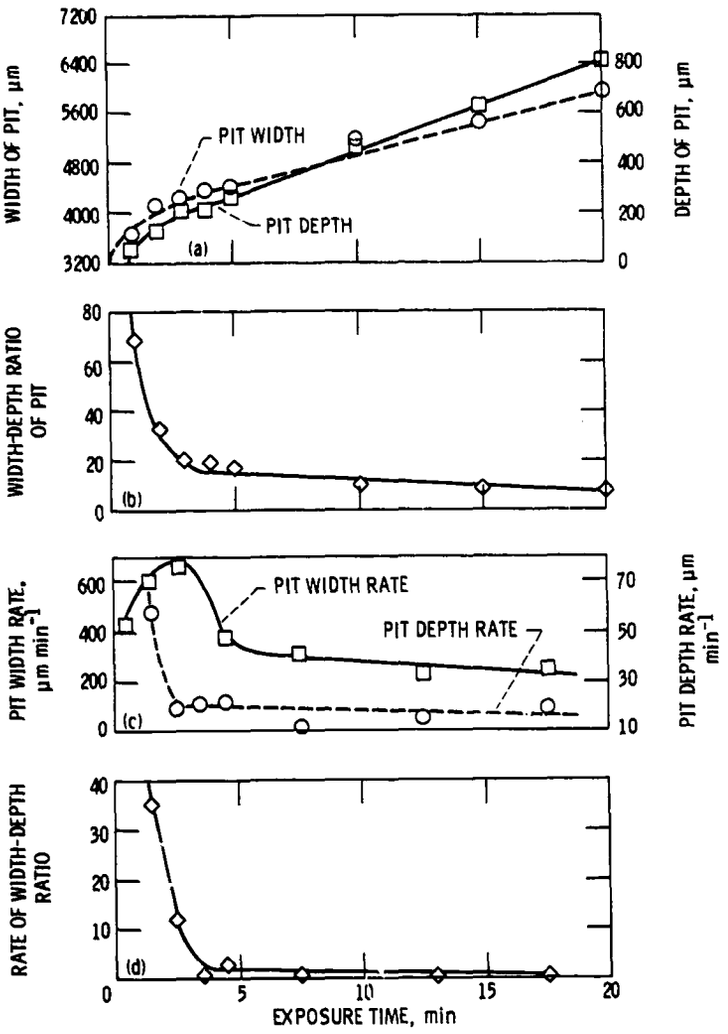

(a) Pit width and pit depth.

(b) Width to depth ratio of pit.

(c) Growth rate of pit width and pit depth.

(d) Growth rate of width to depth ratio of pit.

Figure 3. - Width, depth, and width-depth ratio of pit as a function of exposure time.

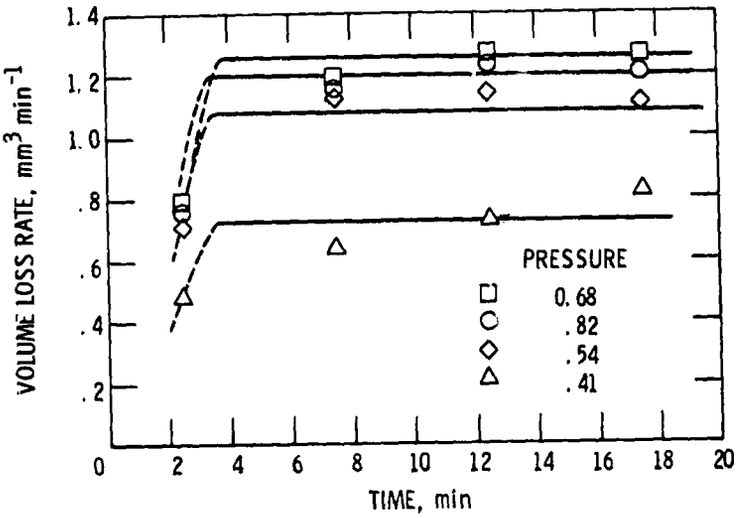

Figure 4. - Instantaneous volume loss rate versus time curves of aluminum alloy at different pressures during glass-bead impingement.

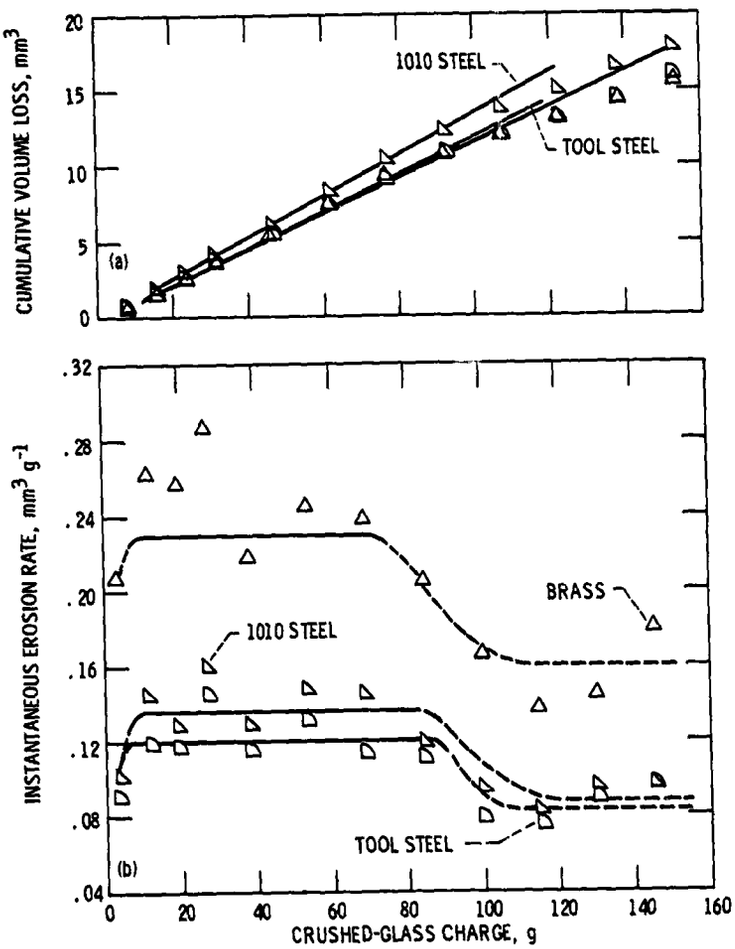

(a) Volume loss.

(b) Volume loss rate.

Figure 5. - Typical erosion-time curves during crushed-glass impingement. Pressure, 0.54 MPa; crushed-glass flow.

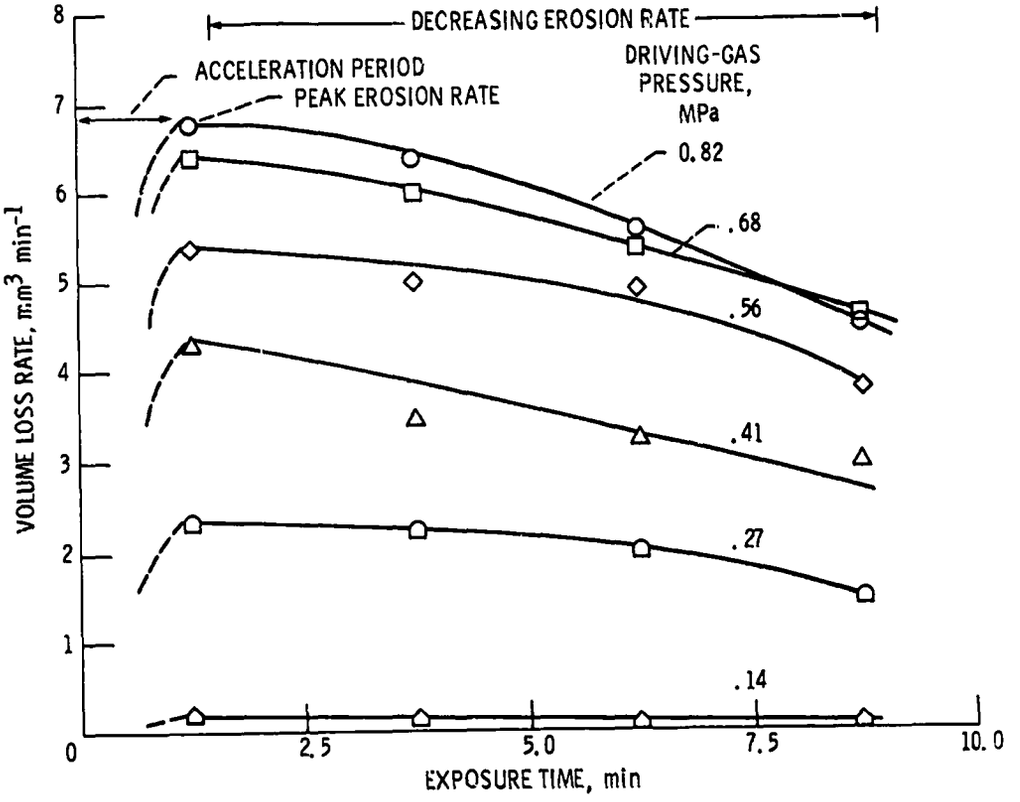

Figure 6. - Instantaneous volume-loss-rate-versus-time curves of aluminum alloy at different pressures during crushed-glass particle impingement.

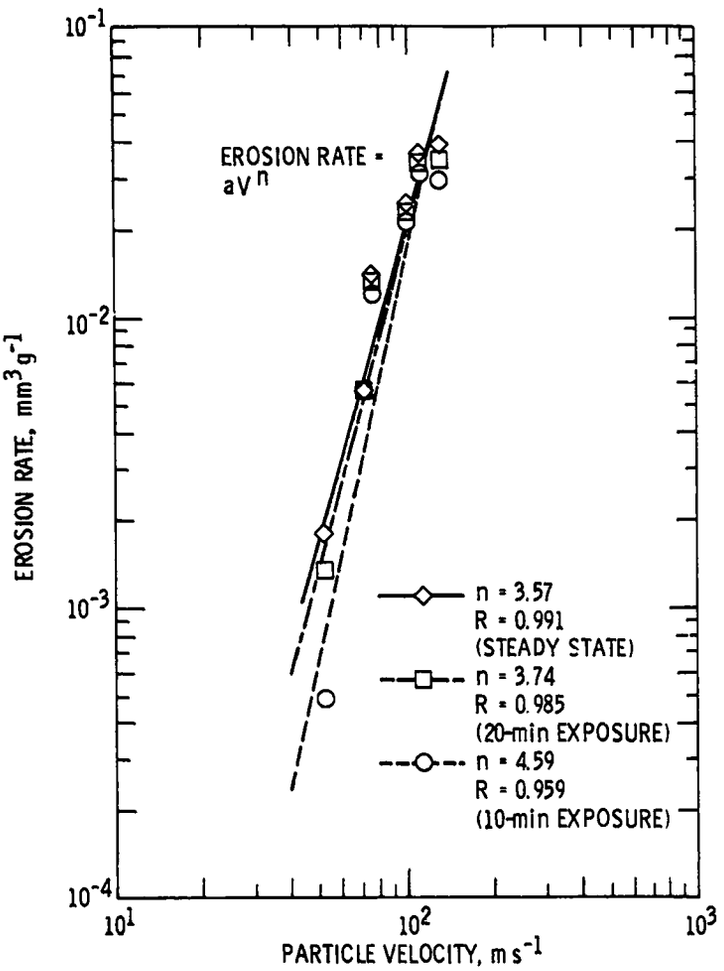

Figure 7. - Normalized erosion rate as a function of particle velocity illustrating the effect of stage of erosion.

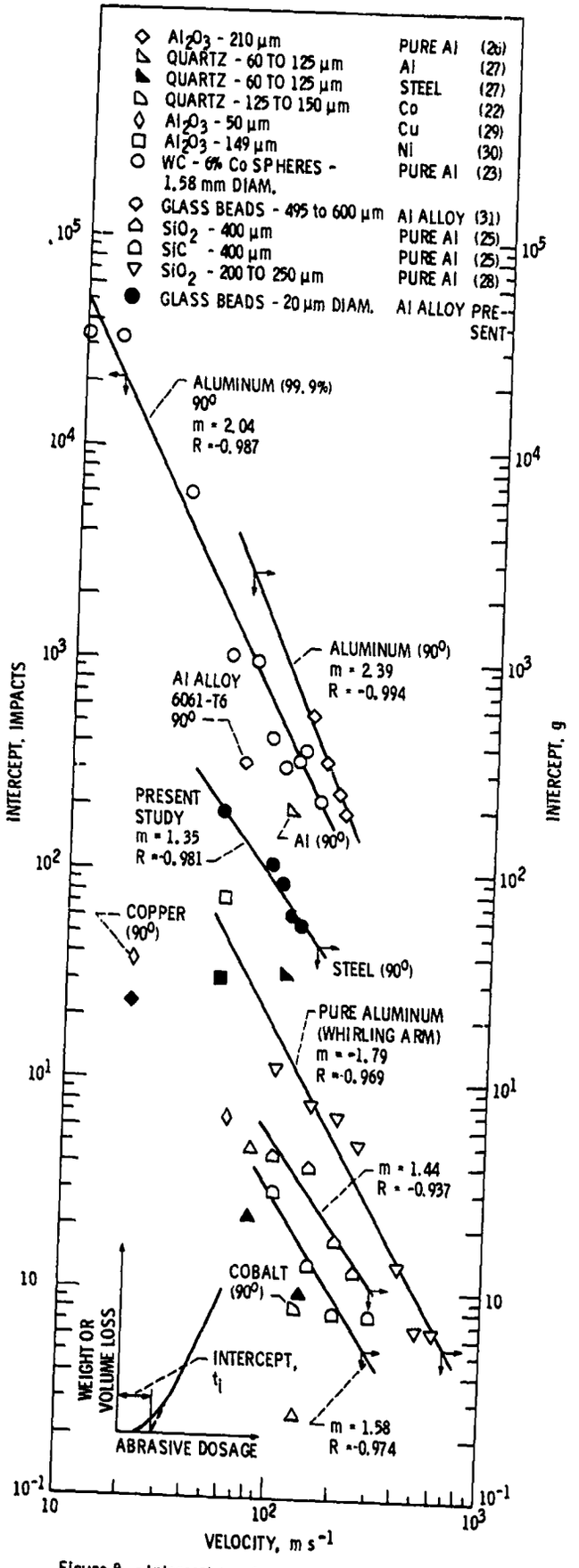

Figure 8. - Intercept as a function of particle velocity.

END

DATE

FILME